IOP Publishing Journal of Physics D: Applied Physics
J. Phys. D: Appl. Phys. **40** (2007) 1839–1844 doi:10.1088/0022-3727/40/7/001

Structural, magnetic and magneto-transport studies on the $(La_{2/3}Sm_{1/3})_{0.67}Ba_{0.33-x}Sr_xMnO_3$ (x = 0, 0.1, 0.2 and 0.33) manganites

Saket Asthana[1] **and D Bahadur**

Department of Metallurgical Engineering and Materials Science, Indian Institute of Technology, Bombay, Powai, Mumbai 400076, India

E-mail: asthanasaket@gmail.com

Received 7 November 2006, in final form 20 December 2006
Published 16 March 2007
Online at stacks.iop.org/JPhysD/40/1839

Abstract
The effect of substituting Sr for Ba on the magneto-transport and magnetic properties of the $(La_{2/3}Sm_{1/3})_{0.67}Ba_{0.33}MnO_3$ system has been investigated. The samples of $(La_{2/3}Sm_{1/3})_{0.67}Ba_{0.33-x}Sr_xMnO_3$ (x = 0.0, 0.1, 0.2 and 0.33) are synthesized by the citrate gel route and crystallize in an orthorhombic structure. The unit cell volume decreases while the metal–insulator transition temperature (T_{MI}) increases with increasing Sr content. The atomic disorder, which is represented by the size variance, increases with Ba content. The small anomaly in $\rho(T)$ due to the atomic disorder which leads to the different magnetic ordering followed by a broad metal–insulator transition is observed in Ba-rich systems. The peak at T^* (small anomaly) is presumed to be due to spin-dependent interfacial tunnelling that causes the difference in magnetic order between the surface and the core. The suppression in the resistivity values with increasing Sr content could be due to the more symmetric MnO_6 octahedra network. The paramagnetic phase coexists with the magnetically ordered phase between T^* ($\sim T_C$) and T_{MI}. The suppression of the metastable magnetic phase leads to the high magnetoresistance in Ba-rich samples. The transport data has been analysed using a small polaron correlated model. The magnetic behaviour may be understood by the Ising model. The overall magnetic behaviour could be accounted for by the competing antiferromagnetic and ferromagnetic interactions.

1. Introduction

The mixed valent perovskite manganites of the general formula $Ln_{1-x}Ae_xMnO_3$ (Ln = rare-earth and Ae = divalent alkaline-earth cation) have created a great deal of interest because of their colossal magnetoresistance (CMR), charge-ordering, electronic phase separation, etc. These systems also have technological importance such as in sensor applications, and especially for increasing data storage by increasing the sensitivity of hard disk drive read heads [1,2]. The manganites can also be prominent candidates for spintronics devices due to their higher spin polarization. These manganites become ferromagnetic (FM) at an optimal value of x (or Mn^{4+} content) and undergo metal–insulator (MI) transition around the ferromagnetic transition temperature. The effects of divalent alkaline-earth element substitution in the stoichiometric perovskite manganites $Ln_{1-x}Ae_xMn_{1-y}M_yO_3$ have been extensively studied [3–5]. These studies show that the Curie temperature, T_C, and the magnetoresistance (MR) are optimized for a Mn^{4+} content of about 33%. These properties are attributed to the double exchange (DE) interaction associated with electron hopping from Mn^{3+} to

[1] Author to whom any correspondence should be addressed.

Mn^{4+}. The double exchange interaction, which favours itinerant electron behaviour, is opposed by the Jahn–Teller (JT) distortion of the Mn^{3+}. Recent studies have shown that DE alone cannot explain the observed behaviour in manganites [6] and other effects are also important. These include the average A-site cationic radius $\langle r_A \rangle$ [7, 8], A-size cationic size mismatch [9, 10], oxygen deficiency [11], electron–lattice coupling [12], polaron effect due to strong electron–phonon interaction arising from the Jahn–Teller distortion [6], etc. The average size of the A-site cation of these perovskites and the size mismatch at the A-site modify the Mn–O–Mn bond angle and affect the e_g electron hopping between the Mn^{3+} and Mn^{4+} degenerate states. The effect of ionic size variation can also be understood by the tolerance factor defined as, $\tau = (\langle r_A \rangle + r_O)/\sqrt{2}(r_B + r_O)$, where r_O and r_B are radii of the oxygen and the B-site transition metal ions, respectively. The A-site cation disorder is responsible for the lattice distortion which leads to the localization of e_g electrons, which in turn leads to electronic phase separation in these materials [13, 14]. The variation in physical properties is generally accounted for by the average size of the A-site cation, $\langle r_A \rangle$, and the size mismatch at the A-site $\sigma^2(r_A)$ which modify the Mn–O–Mn bond angle and affect the e_g electron hopping between the Mn^{3+} and the Mn^{4+} states. The electronic properties of the manganites can be tuned either by substituting cations at the A- or B-sites or by varying the oxygen content in the regular perovskites structure [15, 16].

A comprehensive work has been done on manganites with the single rare-earth ion at the A-site [13, 14]. In the present studies, we have undertaken to substitute two rare-earth ions, namely La and Sm, at the A-site in a fixed ratio and vary the alkaline-earth ion concentration. Sm^{3+} ion (IR = 1.24 Å) is substituted with La^{3+} (IR = 1.36 Å, large variation) to study the effect of A-site ionic radii on the magnetic and magneto-transport properties. Therefore, the series $(La_{2/3}Sm_{1/3})_{0.67}Ba_{0.33-x}Sr_xMnO_3$ ($x = 0$, 0.1, 0.2 and 0.33) has been chosen for the present studies.

2. Experimental details

The polycrystalline samples were synthesized by the chemical citrate-gel route using high purity La_2O_3, Sm_2O_3, $BaCO_3$, $SrCO_3$ and Mn-acetate. The as prepared powders were calcined at 1000 °C in air for 2 h. The powders were pelletized in the form of rectangular bars and sintered at 1200 °C in air. X-ray diffraction patterns of the samples were recorded using Cu-K_α radiation (PW 3040/60 Philips, PANalytical). Resistivity measurements at different applied magnetic fields were carried out from 20 to 300 K using the standard four-probe dc method. Magnetic measurements were made using a vibrating sample magnetometer (LakeShore, 7410) at different fields and in the temperature range 80–300 K.

3. Results and Discussion

Figure 1 shows the x-ray diffraction patterns for $(La_{2/3}Sm_{1/3})_{0.67}Ba_{0.33-x}Sr_xMnO_3$ $x = 0$, 0.1, 0.2 and 0.33) compositions. All the lines in the patterns could be indexed on the basis of an orthorhombic structure (space group *Pnma* No 62). The peaks shift towards higher angle as the

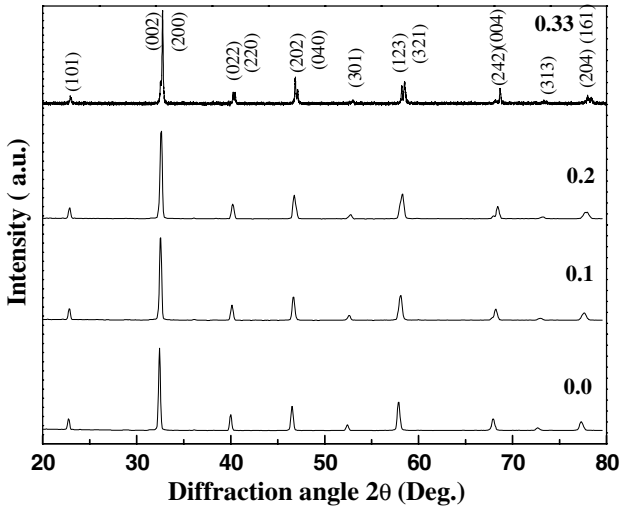

Figure 1. X-ray diffraction patterns of the series $(La_{2/3}Sm_{1/3})_{0.67}Ba_{0.33-x}Sr_xMnO_3$ ($x = 0$, 0.1, 0.2 and 0.33).

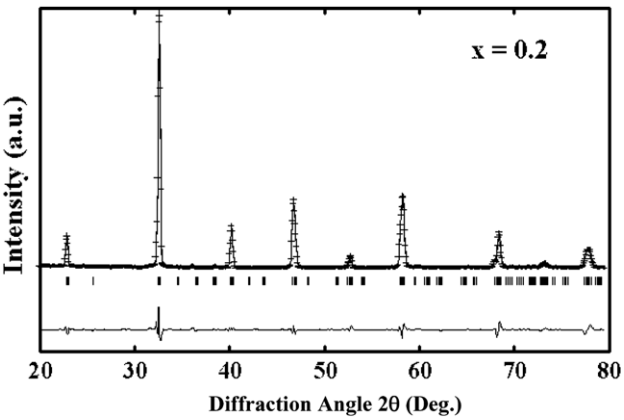

Figure 2. Observed and fitted x-ray diffraction pattern of $(La_{2/3}Sm_{1/3})_{0.67}Ba_{0.23}Sr_{0.2}MnO_3$.

concentration of Sr^{2+} increases. A typical refined pattern of the sample with $x = 0.2$ is shown in figure 2. The average A-site ionic radius $\langle r_A \rangle$ decreases with Sr-substitution due to its smaller ionic size of 1.44 Å as compared with Ba (1.61 Å). The mean radius has been calculated using the coordination number twelve [17]. The tolerance factor is the highest in Ba-substituted samples. This indicates that the structure tends towards pseudo-cubic symmetry as one goes from Sr to Ba substituent. The $\langle r_A \rangle$ varies from 1.42 Å (for $x = 0$) to 1.36 Å (for $x = 0.33$). The cell volume decreases with increasing Sr content as was expected. The percentage of Mn^{4+} has been checked by the idiometric titration and their variation is from 31.6% (for $x = 0$) to 33.2% (for $x = 0.33$). The deviation in the oxygen stochiometry varies from 2.993 (for $x = 0$) to 3.001 (for $x = 0.33$). It confirms the high purity of the compositions.

The cell and structural parameters of these compounds were refined by the Rietveld method using the computer code FULLPROF [18]. The refinement was carried out in the space group *Pnma* (No 62) with the following atomic positions: Ln/A: $4c(x, y, 1/4)$, Mn: $4b(0, 0, 1/2)$, O(1): $4c(x, 1/4, z)$ and 8dO(2): (x, y, z). The oxygen positions derived from the refinement have high errors due to the presence of strong

Table 1. Refined lattice parameters, a, b, c using the Rietveld method and tolerance factor τ for the studied compounds, $(La_{2/3}Sm_{1/3})_{0.67}Ba_{0.33-x}Sr_xMnO_3$ ($x = 0$, 0.1, 0.2 and 0.33).

Composition	a (Å)	b (Å)	c (Å)	V (Å)^3	τ
$x = 0$	5.5312(5)	7.7979(2)	5.5164(8)	237.92(9)	0.9981
$x = 0.1$	5.5196(3)	7.7686(5)	5.4965(6)	235.68(9)	0.9887
$x = 0.2$	5.5149(6)	7.7430(3)	5.4845(8)	234.19(7)	0.9850
$x = 0.33$	5.4962(5)	7.7053(7)	5.4582(8)	231.15(4)	0.9778

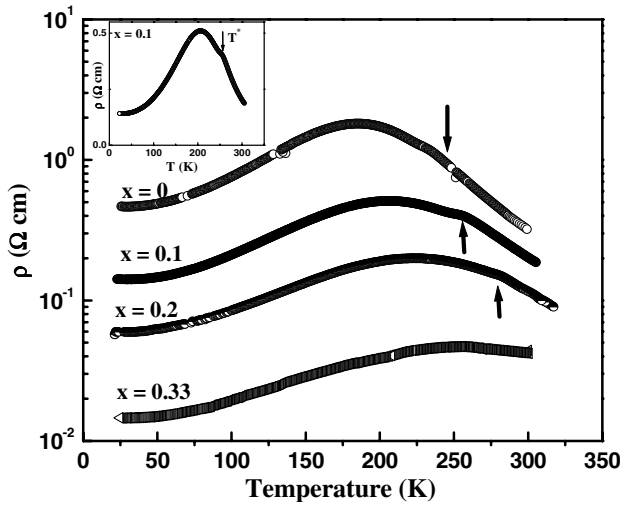

Figure 3. Variation of resistivity with temperature for the series$(La_{2/3}Sm_{1/3})_{0.67}Ba_{0.33-x}Sr_xMnO_3$ ($x = 0$, 0.1, 0.2 and 0.33). The small anomaly for sample with $x = 0.1$ is shown in the inset. Arrows indicate the particular transition, T^*.

scatterers (rare-earth ions) [19]. The best-fit χ^2 values are in the range from 2.89 to 1.12. The refined lattice parameters with tolerance factors are summarized in table 1.

Figure 3 shows the resistivity variation with temperature for the series $(La_{2/3}Sm_{1/3})_{0.67}Ba_{0.33-x}Sr_xMnO_3$ ($x = 0$, 0.1, 0.2 and 0.33). The atomic disorder, which is represented by the size variance, increases with Ba content. The small anomaly in $\rho(T)$ due to the atomic disorder [20] followed by broad metal–insulator transition is observed in Ba-rich systems. The peak at higher temperature in the $\rho(T)$ behaviour could be due to the interfacial tunnelling mechanism. The peak at T_{MI} is a sign that the polarons delocalize to bare carriers and the electrical conduction changes from polaron hopping to free carriers itinerating in a FM environment .The long-range ferromagnetism persists up to a larger extent as the T_{MI} value approaches the T_C value. Therefore, carriers become delocalized from polarons and become mobile and the metallic property enhances. The peak at T^* is presumably believed to be due to spin-dependent interfacial tunnelling arising out of the difference in magnetic order between the surface and the core [21].

The temperature corresponding to the small anomaly is designated by T^*, which is close to the T_C values. T_C is determined by the minima in the dM/dT plots. The $\langle r_A \rangle$ for the sample with $x = 0.33$ is 1.36 Å, which is close to the ionic radius of the oxygen anion (1.35 Å) [22]. This leads to the more symmetric MnO_6 octahedra network within the lattice that in turn suppresses the small transition as well as the resistivity values with increasing Sr^{2+} content.

These samples (especially Ba-rich) are paramagnetic and insulating above T^* and are magnetically ordered and metallic below T_{MI}. This shows that the paramagnetic (PM) phase coexists with the magnetically ordered phase between $T^*(\sim T_C)$ and T_{MI} [20]. The $\langle r_A \rangle$ approaches the ionic radius of oxygen ion with increasing Sr content as a result of which the Mn–O–Mn bond angle approaches 180°. The transfer integral increases with bond angle and results in a resistivity drop.

The transport data has been analysed using a small polaron correlated model [23]. The expression for dc conductivity for small polaron hopping for a temperature greater than $\theta_D/4$ as obtained by Reik based on the Holstein Hamiltonian [24] is

$$\sigma_{hop} = \frac{\sqrt{\pi}}{2} n \left(\frac{b}{\hbar}\right)^2 e^2 a^2 \beta\tau \sec h^2[\varepsilon_p \beta/2] \exp(-U\beta), \qquad (1)$$

where θ_D is the Debye temperature. Here n is the number density of polarons, $\beta = 1/k_B T$, a is the nearest neighbour distance, τ is the relaxation time, b is the transfer integral, U is the activation energy and ε_p is the small polaron stabilization energy. According to Mott, $U = U_H + U_D$ for $T > \theta_D/2$, where U_H denotes the contribution from thermally activated hopping and U_D from the atomic ordering energy. At low temperatures, variable range hopping leading to Anderson localization takes over and for $T \to 0$, σ vanishes as $A\exp(-a/T^{1/4})$. It is shown that equation (1) applies to electrical conductivity in the range $T_V < T < 700$ K in magnetite if $U = 0$ and $(b/h)^2\tau = \omega_{ph}$ with $\varepsilon_p = 0.055$ meV, where T_V is the Verwey transition temperature [25]. This expression could also be applied to manganites if the relaxation time includes both the electron–phonon and the spin–spin relaxation times and $U = U_D$ which is associated with the formation of the magnetic polarons. Since the jump activation energy U_H vanishes in this model it is referred to as the motion of the correlated polarons. U_D can be expressed as $U_0\xi^2$, $\xi = S_a(1 - S_m)\sigma_a$ and $U_0 = (1/4)n_{ph}\omega_{ph}$, where n_{ph} is the average number of phonons in the polaron cloud. Here S_a and σ_a are the long and short range atomic order parameters. In manganites, $S_a = 1$, $S_m = m(t)$ and ξ^2 is equal to $(1 - m^k)\sigma_a^2$. The Debye temperature of the displaced (active mode) phonon which depends on the electron–phonon strength is defined by $\bar{\theta}_D$ [26]. Equation (1) can now be written as

$$\rho_c^{hop} = \frac{AT}{n}[1 + c(1 - m^2(t))\sigma_a^2]\cosh^2(\varepsilon_p/2T) \times \exp[U_0(1 - m^k)\sigma_a^2/T], \qquad T > \bar{\theta}_D/4, \qquad (2)$$

where $m(t) = M(T)/M(0)$, n is the number density of charge carriers and c and k are constants depending on the strength of the spin–spin scattering in polaron transport. Here $A = 2k_B/\sqrt{\pi}\omega_{ph}a^2e^2$, ω_{ph} is the frequency of the active phonon, a is the lattice constant and σ_a varies with T as $(1\text{-}0.75t_{ca}^3)^{1/2}$, where $t_{ca} = T/T_{ca}$. Equation (2) is similar to that obtained for glassy

semiconductor ($m(t) = 0$) by Mott [27] for $T > \bar{\theta}_D/4$. For $T < \bar{\theta}_D/4$, quantum effects dominate over classical effects and according to Mott, due to processes like variable range hopping and Anderson localization, as T tends to zero, ρ increases as $A' \exp(b/T^{1/4})$. This is clearly not applicable to manganites where for the same number of charge carriers (x = constant) and nearly identical room temperature resistivity, the residual resistivity, $\rho(0)$, changes from 2 mΩ cm to 10^3 Ω cm, six orders of magnitude, when $\langle r_A \rangle$ is varied [14]. The residual resistivity follows the proportionality relation with $\cosh^2(2\varepsilon_p/\bar{\theta}_D)$, where ε_p is the polaron energy in equation (2).

Scattering by phonons is proportional to lattice strain $\langle \delta R^2 \rangle / R^2$, which is equal to $1.6 k_B T/Ms^2$ in the high temperature limit where phonons dominate and to $0.4 k_B \bar{\theta}_D/Ms^2$ in the low temperature limit where zero point vibrations dominate. Here M is the mass of the ion and s is the velocity of sound [28]; following Mott, equation (2) gives the resistivity for $T < \bar{\theta}_D/4$ by replacing T by $\bar{\theta}_D/4$ in the prefactor and in the cosh term, because the statistical weight of each lattice vibrational mode in the electron–phonon scattering due to zero point vibration is the same. Then equation (2) becomes

$$\rho_c^{\text{hop}} = \frac{A\bar{\theta}_D}{4n}[1 + c(1 - m^2(t))\sigma_a^2] \cosh^2(2\varepsilon_p/\bar{\theta}_D) \times \exp[4U_0(1 - m^k)\sigma_a^2/\bar{\theta}_D], \qquad T > \bar{\theta}_D/4. \tag{3}$$

For $T \to 0$ using $c = 1$ and spin-wave theory,

$$\rho_c^{\text{hop}} = \rho(0)[1 + 2\zeta T^{3/2}\sigma_a^2], \tag{4}$$

where ζ is the spin-wave constant and

$$\rho(0) = \frac{A\bar{\theta}_D}{4n} \cosh^2\left(\frac{2\varepsilon_p}{\bar{\theta}_D}\right). \tag{5}$$

With the same parameters A/n, T_c, T_{ca}, $\bar{\theta}_D$, U_0 and $k = 2.3$, $\rho(T)$ is plotted using the high temperature (equation (2)) and the low temperature (equation (3)) limits. T_{ca} is taken to be 310 K which is fixed throughout the series. First ε_p is estimated from the high-T plot, then $\bar{\theta}_D$ is estimated using equation (5).

The experimental $\rho(T)$ is fitted using the high temperature (equation (2)) and the low temperature (equation (3)) limits with the fixed parameters $k = 2.3$ and $T_{ca} = 310$ K. Here, the residual resistivity value is taken as the value at 25 K due to experimental constraints instead of 0 K. The experimental as well as fitted plots are shown in figure 4 and parameters are given in table 2.

ε_p is related to the depth of the potential well which localizes the electron and $\bar{\theta}_D$ is the strength of the lattice vibrations that delocalizes the charge carriers so mobility $\mu\alpha \text{sech}^2[\varepsilon_p/2(\bar{\theta}_D/4)]$ as $T \to 0$ where zero point vibrations dominate. The sample with $x = 0.33$ has the lowest ε_p and the highest $\bar{\theta}_D$ value among the series (table 2). Therefore, the resistivity value is the least in this sample due to the highly itinerant character of the charge carriers.

The number of charge carriers increases with Sr content and it is five times greater in sample with $x = 0.33$ form the Ba-rich samples. ε_p, which is the energy required for small polarons to hop between adjacent sites, varies from 310 K (for $x = 0.33$) to 400 K (for $x = 0$) and is nearly constant for Sr-containing samples throughout the series . It reflects in the resistivity value variation which is almost invariable with Sr substitution. The systematic drop in the thermally assisted activation energy is observed as the system varies from $x = 0$ to $x = 0.33$. The small deviation (~0.01 Ω cm) in theoretical fit from the experimental data is observed in the sample with $x = 0.33$ at low temperature.

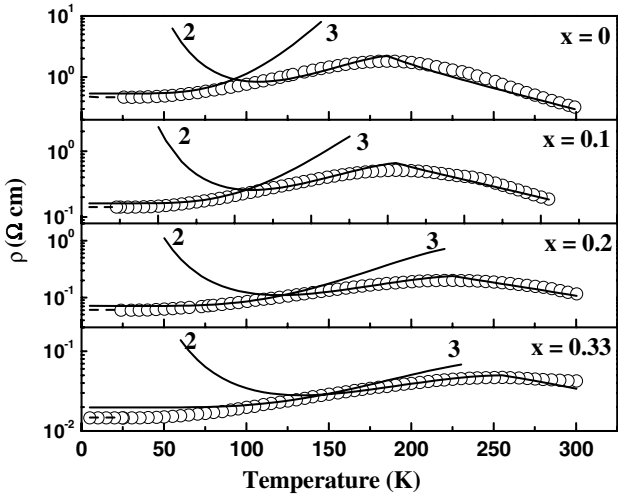

Figure 4. Observed $\rho(T)$ curves for $(La_{2/3}Sm_{1/3})_{2/3}Ba_{1/3-x}Sr_xMnO_3$ ($x = 0$, 0.1, 0.2 and 0.33) are shown in hollow circles. The fitted plots are shown by solid lines for the low temperature (equation (3)) and the high temperature (equation (2)) limit.

Figure 5 shows the magnetoresistance behaviour of the samples of series $(La_{1/3}Sm_{2/3})_{0.67}Ba_{0.33-x}Sr_xMnO_3$ ($x = 0$, 0.1, 0.2 and 0.33) in an applied field of 8.5 kOe. In the presence of an external field, the resistivity decreases significantly. An intuitive view on the MR effect is that the magnetic field tends to align the local spins, and the forcedly spin-polarized conduction electron suffers less from the scattering by local spins and becomes more itinerant. The MR is defined as

$$\%\text{MR} = 100 \times [\rho(H, T) - \rho(0, T)]/[\rho(0, T)], \tag{6}$$

where $\rho(H, T)$ and $\rho(0, T)$ are the resistivities at a temperature T, in an applied magnetic field H and in a zero applied magnetic field, respectively.

The small anomaly in the vicinity of T_C in resistivity disappears in magnetic fields of 8.5 kOe as shown in the inset by an arrow. The small jump is observed in the negative percentage of MR variation plots particularly at temperature T^* especially in samples with $x = 0$ and 0.1. It indicates the presence of metastable spin states, which vanishes even in small magnetic fields. The two different kinds of MR behaviour, one at around T_{MI} due to intergrain tunnelling and the other at T^* due to spin dependent tunnelling, are observed in Ba-rich samples [20]. The MR value increases with the atomic disorder and a maximum (~22% at 100 K) is observed for the sample with $x = 0$. The conduction mechanism in the vicinity of T^* (~T_C) could be explained by the magnetic polaron formation. The spin of a conducting electron induces a local distortion of the spin lattice and moves on surrounded by this spin polarization [29]. The peak in the MR around T^* could be due to the inhibition of magnetic polaron formation in an applied magnetic field that results in a prominent MR effect [30].

The variation of magnetization with temperature for the series $(La_{2/3}Sm_{1/3})_{0.67}Ba_{0.33-x}Sr_xMnO_3$ ($x = 0$, 0.1,0.2 and

Table 2. The fitted parameters, ε_p, $\bar{\theta}_D$, U_0 and n are given for the series $(La_{2/3}Sm_{1/3})_{2/3}Ba_{1/3-x}Sr_xMnO_3$ ($x = 0$, 0.1, 0.2 and 0.33). The value of A/n has been obtained from the $\rho(0)$ values using ω_{ph} with $a = 3.858$ Å. The maximum percentage of MR in 8.5 kOe fields, T_{MI}, T^* and T_C are also included.

x	A/n (10^{-4}/cc)	ε_p (K)	$\bar{\theta}_D$ (K)	U_0 (K)	n ($\times 10^{20}$/cc)	σ^2 (rA) ($\times 10^{-3}$Å^2)	T_{MI} (K)	T^* (K)	T_C (K)	% MR_{max}
0	3	400	370	460	2.5	18.6	186	235	240	∼25
0.1	2.6	330	430	360	3	12.6	206	256	260	∼20
0.2	1.5	320	470	330	5	7.8	225	282	280	∼20
0.33	0.5	310	590	230	15	3.2	∼256	—	340	∼15

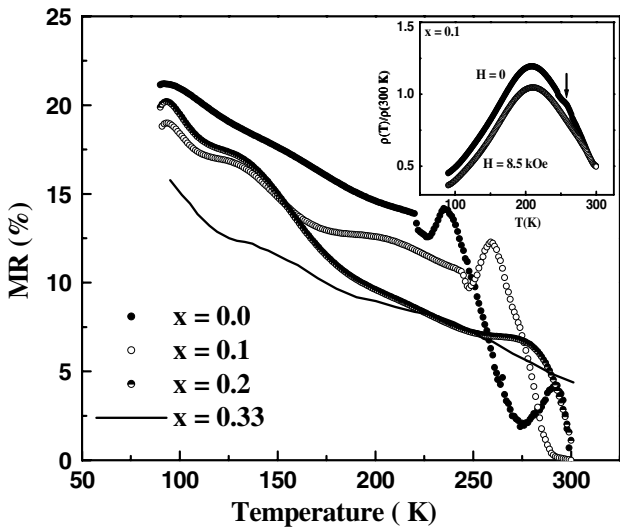

Figure 5. Variation of percentage of MR with temperature for series $(La_{2/3}Sm_{1/3})_{0.67}Ba_{0.33-x}Sr_xMnO_3$ ($x = 0$, 0.1, 0.2 and 0.33) in 8.5 kOe field. Inset shows the $\rho(T)$ behaviour for sample with $x = 0.1$ in field and without field.

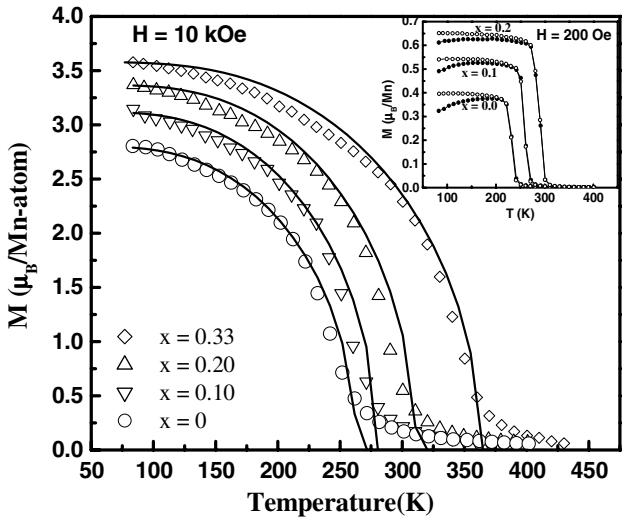

Figure 6. Variation of magnetization with temperature in 10 kOe fields for the series $(La_{2/3}Sm_{1/3})_{0.67}Ba_{0.33-x}Sr_xMnO_3$ ($x = 0$, 0.1, 0.2 and 0.33). Inset shows the M–T plot for $x = 0$, 0.1, 0.2 measured in a field of 200 Oe. Solid lines show the fitted plots obtained by using the Ising model.

0.33) in 10 kOe fields is shown in figure 6. The inset shows the thermal irreversibility behaviour in zero field cooled (ZFC) and field cooled (FC) plots due to the competing antiferromagnetic (AFM) and FM interaction for samples with $x = 0$, 0.1 and 0.2 in 200 Oe fields. The irreversibility increases with Ba

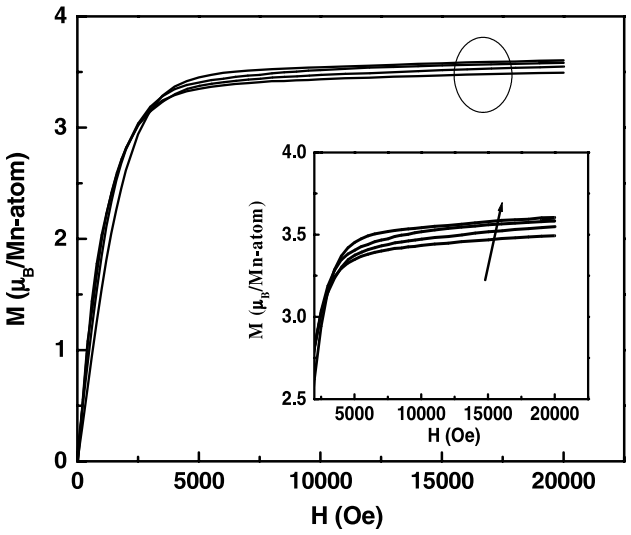

Figure 7. The isothermal magnetization plots of the series $(La_{2/3}Sm_{1/3})_{0.67}Ba_{0.33-x}Sr_xMnO_3$ ($x = 0$, 0.1, 0.2 and 0.33) at 80 K. Arrow in the inset indicates the increasing Sr^{2+} content.

content due to increasing size disorder, which is also observed in MR and transport studies. The T_C as well as magnetic moment increases with the Sr content. It indicates that the long-range ferromagnetic effect also becomes prominent with the Sr content.

The magnetization behaviour of all the samples agrees well with the Ising model, which is described as

$$m = \tanh(m/t). \tag{7}$$

Here m is the reduced magnetization $M(T)/M(0)$ and t is the reduced temperature T/T_C. This is a crude approximation because the local inhomogeneities that are present in the frustrated systems play an important role. The theoretical fit is shown as solid lines in figure 6. The T_C for the fitting is obtained from the intercept at the x-axis. The theoretical fit to $M(T)$ data shows that the molecular field approximation with $s = 1/2$ is applicable. As temperature increases the magnetization decreases smoothly to zero at $T = T_C$. This behaviour classified the usual FM/PM transition as a second order transition. The width of the transition increases with increasing Sr content.

Figure 7 shows the isothermal magnetization field plots of the series $(La_{2/3}Sm_{1/3})_{0.67}Ba_{0.33-x}Sr_xMnO_3$ ($x = 0$, 0.1, 0.2 and 0.33). All the samples exhibit non-saturation in magnetization even though their maximum magnetic moment approaches the theoretical value of 3.7 μ_B/Mn. The enlarged view of the non-saturation is shown in the inset. This non-saturating M–H behaviour may be attributed to the

suppression of double exchange due to decreasing Mn–O–Mn bond angle with decreasing Sr content. The possibility of spin canting could not be ruled out in Ba-rich samples due to the presence of disorder. The non-saturating isothermal magnetization in Ba containing samples is evident from competing antiferromagnetic (SE) and ferromagnetic (DE) interactions which leads to frustration in these systems [31].

4. Conclusions

All the compounds crystallize in the orthorhombic crystal structure. The T_{MI} shifts to a higher temperature with increasing Sr content due to the suppression of distortion in MnO_6 octahedra as the average A-site ionic size approaches the oxygen ionic size. The transport data is explained by the small polaron correlated model. The two peaks observed in the $\rho(T)$ plots are due to intergrain and interfacial conduction (metastable magnetic phase), respectively, with increasing temperature. The high MR (∼22%) value in the Ba-rich samples is observed due to the destabilization of the metastable magnetic phase that exists between the two peak temperatures. Bifurcation behaviour in the magnetization versus temperature due to the presence of frustration is observed in the ZFC and FC magnetization plots and it decreases with Sr content. The magnetic behaviour may be understood by the Ising model. The non-saturating M–H behaviour is indicative of frustration in the Ba-rich samples due to competing AFM and FM interactions. The overall magnetic and transport properties could be attributed to the competing AFM and FM interactions present in these frustrated systems.

References

[1] Heremans J 1993 *J. Phys. D: Appl. Phys.* **26** 1149
[2] Jin S, McCormack M, Tiefel T H and Ramesh R 1994 *J. Appl. Phys.* **76** 6929
[3] Srivastava C M, Banerjee S, Gundu Rao T K, Nigam A K and Bahadur D 2003 *J. Phys.: Condens. Matter* **15** 2375
[4] Verma D, Nigam A K, Gundu Rao T K and Bahadur D 2004 *J. Magn. Magn. Mater.* **271** 172
[5] Das D, Raj M R, Srivastava C M, Bahadur D, Nigam A K and Malik S K 2004 *J. Phys.: Condens. Matter* **16** 6213
[6] Millis A J, Littlewood P B and Shraiman B I 1995 *Phys. Rev. Lett.* **74** 5144
[7] Mahesh R, Mahendiran R, Raychaudhuri A K and Rao C N R 1995 *J. Solid State Chem.* **114** 297
[8] Damay F, Martin C, Martin A and Raveau B 1997 *J. Appl. Phys.* **81** 1372
[9] Rodriguez-Martinez L M and Attfield J P 1996 *Phys. Rev.* B **54** 15622
[10] Damay F, Martin C, Maignan A and Raveau B 1997 *J. Appl. Phys.* **82** 6181
[11] Troyanchuk I O, Trukhanov S V, Szymezak H and Baerner K 2000 *J.Phys.: Condens. Matter* **12** L155
[12] Millis A J 1997 *J. Appl. Phys.* **81** 5502
[13] Tokura Y 2000 *Colossal Magnetoresistive Oxides* (Amsterdam: Gordon and Breach)
[14] Rao C N R and Raveau B 1998 *Colossal Magnetoresistance, Charge Ordering and Related Properties of Manganese Oxides* (Singapore: World Scientific)
[15] Sudheendra L and Rao C N R 2003 *J.Phys.: Condens. Matter* **15** 3029
[16] Das D, Chowdhury P, Das R N, Srivastava C M, Nigam A K and Bahadur D 2002 *J. Magn. Magn. Mater.* **238** 178
[17] Shannon R D 1976 *Acta Crystallogr.* A **32** 751
[18] FULLPROF 2001 http://www-llb.cea.fr/fullweb/powder.htm/
[19] Collado J A, Frontera C, Garcia Munoz J L, Ritter C and Brunelli M A G 2003 *Chem. Mater.* **15** 167
[20] Xianyu W-X, Li B-H, Qian Z-N and Jin H-M 1999 *J. Appl. Phys.* **86** 5164
[21] Pi L, Zheng L and Zhang Y 2000 *Phys. Rev.* B **61** 8917
[22] Asthana S, Bahadur D, Nigam A K and Malik S K 2005 *J. Appl. Phys.* **97** 10H711
[23] Srivastava C M 1999 *J. Phys.: Condens. Matter* **11** 4539
[24] Reik H G 1972 *Polarons in Ionic Crystals and Polar Semiconductors* ed J T Devreese (Amsterdam: North-Holland) pp 679–714
[25] Srinivasan G and Srivastava C M 1981 *Phys. Status. Solidi.* b **103** 665
[26] Asthana S, Bahadur D and Srivastava C M 2006 *Physica* B **371** 241
[27] Mott N F and Davis E A 1979 *Electronic Processes in Non-crystalline Materials* 2nd edn (Oxford: Clarendon)
[28] Pines D 1964 *Elementary Excitations in Solids* (New York: Benjamin)
[29] Kusters R M, Singleton J, Keen D A, McGreevy R and Hayes W 1989 *Physica* B **155** 362
[30] Rao G H, Sun J R, Sun Y Z, Zhang Y L and Liang J K 1996 *J. Phys.: Condens. Matter* **8** 5393
[31] Asthana S, Bahadur D, Nigam A K and Malik S K 2004 *J. Phys: Condens. Matter* **16** 5297